Conformational dynamics of human Protein Kinase CK2α and its effect on function and inhibition

Ashutosh Srivastava[1], Tsuyoshi Hirota[1,2], Stephan Irle[1], Florence Tama[1,3,4]

[1]Institute of Transformative Bio-Molecules (WPI-ITbM), Nagoya University, Nagoya, Japan

[2]PRESTO, JST, Nagoya, Japan

[3]Graduate School of Science, Department of Physics, Nagoya University, Nagoya, Japan

[4]Computational Structural Biology Research Unit, RIKEN Advanced Institute of Computational Science, Kobe, Japan

Corresponding Author:

Florence Tama

Institute of Transformative Bio-Molecules (WPI-ITbM), Nagoya University, Nagoya, Japan

Email- florence.tama@nagoya-u.jp

Short title- Conformational dynamics of Protein Kinase CK2

Keywords- CK2, Molecular dynamics, Principal Component Analysis, Dynamic Equilibrium, Crystal Structure Ensemble

Abstract

Protein Kinase CK2 is ubiquitously expressed and highly conserved protein kinase that shows constitutive activity. It phosphorylates a diverse set of proteins and plays crucial role in several cellular processes. The catalytic subunit of this enzyme (CK2α) shows remarkable flexibility as evidenced in numerous crystal structures determined till now. Here, using analysis of multiple crystal structures and long timescale molecular dynamics simulations, we explore the conformational flexibility of CK2α. The enzyme shows considerably higher flexibility in the solution as compared to that observed in crystal structure ensemble. Multiple conformations of hinge region, located near the active site, were observed during the dynamics. We further observed that among these multiple conformations, the most populated conformational state was inadequately represented in the crystal structure ensemble. The catalytic spine, was found to be less dismantled in this state as compared to the "open" hinge/αD state crystal structures. The comparison of dynamics in unbound (Apo) state and inhibitor (CX4945) bound state exhibits inhibitor induced suppression in the overall dynamics of the enzyme. This is especially true for functionally important Glycine – rich loop above the active site. Together, this work gives novel insights into the dynamics of CK2α in solution and relates it to the function. This work also explains the effect of inhibitor on the dynamics of CK2α and paves way for development of better inhibitors.

Introduction

Phosphorylation of proteins is one of the most important regulatory phenomenon, playing crucial role in almost all cellular processes. The enzymes catalyzing phosphorylation reaction, referred to as protein kinases, form one of the largest protein super-families in human[1]. The protein kinase, CK2 (Casein Kinase II), is a ubiquitously found and highly conserved kinase in eukaryotic organisms. CK2 has a very broad specificity with close to 300 substrates[2] and unlike most of the other protein kinases, it remains constitutively active[3]. Consistent with its role in cell proliferation and apoptosis[4], overexpression of CK2 has been found to be related with tumorigenesis[5, 6]. This makes CK2 a pertinent drug target for anti-cancer therapy[7]. Consequently, considerable efforts have been made to develop small molecule inhibitors against this enzyme[8].

Within cells, CK2 exists as a heterotetramer with two subunits of CK2α/α' (catalytic subunit) and two subunits of CK2β (regulatory subunit)[9]. The regulatory subunit, though important for the function of CK2, has been known to play a role in modulation of the CK2α catalytic activity rather than as a molecular switch turning the activity on or off. This is also evident from the fact that the isolated CK2α has been shown to be catalytically active [9, 10]. Comparison of the isolated CK2α structures and in complex with CK2β further show that there is little effect of CK2β binding on the structure of CK2α, particularly in the active site region. However, binding of CK2β might have allosteric effect on the active site dynamics of CK2α[11]. The inhibitors of CK2 discovered so far, primarily belong to the category of competitive inhibitors, that target the catalytic subunit CK2α and bind to the co-substrate (ATP or GTP) binding site with high affinity. A major deterrent, in targeting the active site to inhibit CK2, is the low specificity of the inhibitors leading to off-target effects due to conserved nature of kinase active sites. Currently, only one molecule (CX-4945), showing high specificity, has

reached the clinical stages[12]. Recently, novel molecules and fragments have been discovered that target either the CK2α-β interface[13], or other sites in conjunction with the active site[14, 15].

The structure of CK2α comprises of two domains and the active site lies at their interface (Figure 1B). It remains constitutively active owing to the peculiar structural features, which cause the activation segment and the helix αC to always be primed for reaction. Numerous studies have been undertaken to investigate the structure-function relationship of CK2 and its inhibition[16–18]. More than a hundred structures of the Protein Kinase CK2α in different complex states and from different organisms, have been deposited in the Protein Data Bank. Based on this extensive structural evidence gathered overtime, it has been reasoned that the inherent conformational plasticity in CK2α plays role in the regulation of this enzyme. This becomes further intriguing when comparing the ortholog of CK2α from maize, which, although sequentially and structurally remarkably similar, shows differences in the conformational flexibility[19]. Based on multiple high resolution structures, crucial differences in the flexibility of the human and maize CK2α, particularly in the αD helix and surrounding hinge region, have been observed. Several original and review publications[19–24] have discussed the conformational heterogeneity of CK2α in great detail in the past. However, the dynamics of this enzyme in solution and the role of dynamics in function and inhibition remains elusive[22]. It is increasingly being realized that the proteins and particularly enzymes are much more dynamic in nature with direct implications in function, inhibition and even evolution[25]. This makes it imperative to understand the conformational dynamics of CK2α in solution. Exploring the full conformational heterogeneity of CK2α in solution is important for development of better inhibitors[26]. Molecular dynamics simulations provide an excellent approach to study the dynamics of proteins in solution. With latest advances in software and hardware, microsecond to millisecond scale molecular dynamics of small or medium sized proteins, is being routinely performed [27–30].

Here, we set out to investigate the conformational plasticity of the CK2α as exhibited by numerous crystal structures and more importantly the dynamics of the CK2α in solution. Using a large dataset of human CK2α structures we first explore their conformational heterogeneity. We compare this heterogeneity to the conformational landscape observed in the molecular dynamics simulations. Further, we compare the dynamics observed in MD simulations for the apo[18] and inhibitor bound CK2α[31] and find crucial differences in them. Finally, we observe conformation of the hinge/αD region, distinct from that observed in the hitherto determined crystal structures.

Materials and Methods

Dataset

Human CK2α structures corresponding to uniprot id P68400 were downloaded from Protein Data Bank[32] (http://www.rscb.org). The structures with missing residues except for the terminal regions were rejected. Finally, 70 structures were selected for the analysis (Table S1). The resolution of the structures varied between 1.04 Å - 3.30 Å. The residues present in all 70 structures spanned from 4 to 327. These residues were used for the analysis wherever cross structure comparison was made.

Alignment and Root Mean Square Deviation

Structures in the dataset were aligned using the Fold server at the European Bioinformatics Institute[33] (http://www.ebi.ac.uk/msd-srv/ssm/) and the Root Mean Square Deviation (RMSD) was calculated. Residue wise RMSD was calculated from the aligned structures as per following equation

$$RMSD_i = \sqrt{\frac{1}{n}\sum_{n} \delta_i^2}$$

where, $RMSD_i$ is the RMSD for the Cα of the i^{th} residue. δ_i is the distance between the Cα atom of each of the n structures and reference structure. B-factors associated with the Cα atoms in the individual PDB files were normalized with respect to the highest B-factors thus converting each set into the range between 0 and 1.

Molecular Dynamics Simulation

Molecular Dynamics simulations were performed in Gromacs 5[34]. The crystal structures of Apo CK2α (PDB id 3AT2) and CX4945 bound CK2α (PDB id 3PE1) were used as starting models for the simulation. All water and ethylene glycol molecules were removed from the Apo structure PDB file. In case of CX-4945 bound CK2 structure, three water molecules that were found to be the ordered waters near the inhibitor were retained and rest of the water, sulphate and ethylene glycol molecules were removed. Amber99sb force field was used for the simulation. The force field parameters for CX-4945 were derived using General Amber Force Field[35] in antechamber[36] utility of Amber Tools 14, implemented through ACPYPE[37]. The structures were solvated in a dodecaheron box filled with TIP3P water molecules. Systems were neutralized using counter ions as needed. Energy minimization was performed for the systems until the maximum force on any atom was less than 100 kJ $mol^{-1}nm^{-1}$. The energy minimized systems were then equilibrated in an NVT ensemble for 1ns followed by NPT equilibration of 1ns using Berendsen barostat[38]. This was followed by the 2ns NPT equilibration using Parinello-Rahman barostat[39]. The temperature was maintained at 300 K using the modified Berendsen Thermostat (V-rescale)[40]. The pressure was maintained at 1 bar. Following equilibration, the production run was performed for 200 ns. The time step used was 2fs and the trajectory frames were saved every 5000 steps. Three independent simulations were performed using the same protocol for each system giving a total sampling of 1.2 μs. Before

analysis, the three independent simulation trajectories for each system were concatenated and fitted to the first frame.

Root Mean Square Fluctuation (RMSF), distance and dihedral angles used in the analysis were calculated using the gromacs utilities gmx rmsf, gmx distance and gmx angle respectively. The eigen values and eigen vectors were determined using the gmx covar utility of gromacs and were analysed using the gmx anaeig. Free Energy Landscapes were constructed using the gmx sham and plotted using in-house python scripts.

UCSF-Chimera[41] and VMD[42] were used for molecular visualization and rendering images of protein structures.

Results

CK2α exhibits conformational flexibility in five structural regions

In this work, we have focused on the human CK2α structures obtained from Protein Data Bank (see Materials and Methods). 70 crystal structures were selected for the analysis. The details of these structures have been given in Supplementary Table S1. The overall root mean square deviation (RMSD) between all the structures was quite low (0.81 Å). RMSD is an average measure that quantifies the overall difference between the structures, thus overlooking the local variations in the structure. To understand the local variations among the structures we calculated residue wise RMSD between the structures. The residue wise RMSD for the ensemble of crystal structures shows high conformational variability in five regions described as 1) Gly rich p-loop, 2) β3/ αC loop, 3) β4-β5 region, 4) Hinge/αD region comprising of αD helix with the inter domain region that connects the C-terminal domain and N-terminal domain and 5) the αGH2 helix far from the active site region. (Figure 1).

This conformational flexibility also becomes evident in the B-factors of the structures. There are five regions (excluding the termini) that show high B factors across most of the

structures (Figure S1). These regions correspond to the five regions described above. A similar observation was made previously by Niefind et. al. [20] using CK2α structures from maize, rat and human, and comparing them to human CDK2 structures.

The conformation of Gly-rich loop (residues- 46-51, green shaded region in Figure 1A and B) shows large variation among different structures. There are two extreme conformations that can be observed among hitherto determined crystal structures. In the stretched conformation, the Gly-rich loop is stretched with Arg 47 side chain pointing upwards leaving the active site open. In the collapsed conformation, the Gly-rich loop is bent downwards with the side chain of Arg 47 blocking the active site (Figure 2A). In a recent computational study[21], the free energy of these two states was found to be similar and the highest free energy barrier in transition between these states was found to be low (~3 kcal/mol). In spite of this fact, out of 70 structures analyzed in the current study, only 2 structures exhibit collapsed Gly-rich loop (PDB: 3FWQ and 4IB5) and in both of these structures the ATP binding region does not contain any ligand. Another atypical conformation of Gly-rich loop was observed in the crystal structure of CK2α solved in high salt conditions and presence of ligand that contributes to a π-halogen interaction causing this conformation[43].

The β3/αC region (residues 70-74, tan shaded region in Figure 1A and B) is shortened in the case of CK2α due to missing αB helix, as compared to other kinases. Considering the structural data available so far, no specific reason has been ascribed to the high flexibility observed in this region (Yellow region in Figure S1B). Recently, in a structure in complex with the CK2β competitive peptide, one of the CK2α chains in asymmetric unit had a cis Pro72 as compared to trans Pro72 found in all other structures[13]. However, significance or role of this cis-trans isomerization could to be determined.

The region surrounding β4/β5 loop (residues 96-113, orange shaded region in Figure 1A and B) forms the interface between the CK2α and CK2β. High flexibility in this region has been attributed to the regulation of CK2β binding and it has been suggested to act as a hinge in this interaction[44]. In the crystal structures analyzed here, two states of this loop can be observed corresponding to the bent and stretched conformation (Figure S1B). However, no correlation can be made to the functional states of the enzyme owing to lack of consistency in the conformation of this region in different holoenzyme (CK2α-CK2β complex) structures

In earlier studies, two distinct states have been defined for the hinge/αD region (cyan (residues 114-118) and purple (residues 121-128) shaded region in Figure 1A and B), referred to as "Open and "Closed" states depending primarily on the orientation of Phe121 side chain. In order to understand the relative representation of these two states in the dataset analyzed here we mapped all the crystal structures in a plane comprising of distance between center of masses (COM) of Phe121 and Val162 (henceforth called dist121-162) as X-axis and C-Cα-Cβ-Cγ dihedral angle of Phe121 (henceforth called dihed121) as Y axis (Figure 2B). A large variation can be observed in dihed121 and the side chain of Phe121 seems to sample three ranges primarily. Phe 121 residues with dihed121 in the range of 25°-75° are buried within hydrophobic cavity, whereas those with values -25° to -75° are exposed on the surface. The distance between COMs of Phe121 and Val162, representing the distance between the αD and β7 clearly distinguishes the open state and closed state structures. Apart from these predominant orientations there are few structures that exhibit extreme values. Previous studies have alluded to different conformations exhibited by the hinge/αD region of human CK2α owing to its relevance to the function and inhibition of this enzyme[19, 45]. In an earlier comprehensive study, Klopffleisch et. al. [45] determined CK2α-resorufin structure in a low density crystal packing state and compared it to other crystal structures both in high density

packing state and low density states to delineate the effects of crystal contacts on the hinge/αD conformation. This study convincingly revealed that external factors like ligand, pH, temperature etc might play a crucial role in defining the conformation of hinge/αD region. It also suggested an existence of dynamic equilibrium between different conformations of hinge/αD region in solution, which might shift due to these external factors. Thus, any efforts in the past to correlate different hinge/αD conformations observed in CK2α to the function of the enzyme have failed except for perhaps one precept that the conformation observed in the crystal structure is dependent on the crystallization conditions and nature of the ligand in the active site[26, 43] . The presence of high concentrations of kosmotropic salts in the crystallization buffers causes the hydrophobic interactions to be dominant and in turn shifts the structures to a closed like conformation.

The αGH2 helix (gray shaded region in Figure 1A and B) is a part of the CMGC family like insert in the CK2α structure. This helix evinces high B-factors and variability among the crystal structures analyzed here, however, no functional role has been ascribed to it yet.

From the above-mentioned analysis, we can conclude that the conformational flexibility is an intrinsic and important feature of CK2α however the role of this flexibility in the function and inhibition remains largely unknown. Although, numerous crystal structures along with the B-factors, give some indication towards the flexibility of the structure, the conformational dynamics of this enzyme in solution remains unexplored. To this end, we performed molecular dynamics simulations of CK2α subunit in explicit solvent in both unbound and inhibitor (CX-4945) bound states. CX-4945 is a benzonaphthyridine derivative that competitively inhibits CK2α with high specificity[12]. The structure of CK2α in complex with CX-4945 (PDB 3PE1) is very similar to the Apo structure (PDB 3AT2) (Cα RMSD of 0.58 Å) and expectedly shows open type conformation of the hinge/αD region and stretched Gly-rich loop[31] (Figure 3A). In the present work, we investigated the dynamics of unbound

CK2α (hereafter ApoCK2α) and compared it with that of the CX-4945 bound CK2α (hereafter CXCK2α) in explicit solvent conditions.

Three independent simulations of 200 ns for each system were performed giving a total sampling time of 1.2 μs. The trajectories obtained from three independent runs were concatenated giving structural snapshots for equilibrium dynamics of 600 ns for each system.

Apo –structure shows higher flexibility than the inhibitor bound structure

Root Mean Square Fluctuation (RMSF) measures the flexibility of the molecule during the dynamics. We calculated the RMSF for the Cα atoms of each residue over the course of the trajectory (Figure 3B). For both, ApoCK2α and CXCK2α, higher flexibility was observed for the variable regions described in the crystal structure ensemble analysis (Figure 1A).

ApoCK2α exhibits higher flexibility as compared to CXCK2α at almost all the residues suggesting inhibitor induced suppression of dynamics in CK2α. There is a considerable decrease in the flexibility in CXCK2α at and near the Gly rich loop (residues- 46-51, Figure 3B green shaded region). The suppression in dynamics of molecule upon binding of inhibitor has been observed previously in other enzymes[46, 47]. This suppression in dynamics is often concomitant with the shift in dynamic equilibrium of conformational states and stabilization of a particular state.

To further explore the difference in the dynamics of the systems and conformational states explored by the enzyme in solution, 2D free energy landscapes (FEL) were generated using the reaction coordinates (RC) corresponding to the Gly-rich loop and hinge/αD conformations.

Inhibitor stabilizes the stretched state by shifting the Gly-rich loop dynamic equilibrium

The distance between the COMs of Arg47 and His 160 (henceforth dist47-160) was chosen as the first RC (RC1) while the dihedral angle formed by Arg47 (Cβ- Cα-C-) – Gly48(N) (henceforth dihed47-48) was chosen as second RC (RC2). The FEL in case of ApoCK2α reveals two minima corresponding to two different distances along RC1 (Figure 4A). The first and deeper minimum, at the lower distance of approximately 6-8 Å corresponds to the collapsed conformation of the Gly rich loop whereas the second comparatively shallow minimum at the distance of approximately 12-14 Å corresponds to the stretched conformation of the loop. Instead, in case of CXCK2α, the FEL displays a single minimum corresponding to the stretched conformation (Figure 4B). This suggests that the ApoCK2α exists in a dynamic equilibrium between the collapsed and stretched Gly-rich conformations. We hypothesize that the inhibitor binds to the CK2α in the stretched conformation and stabilizes it. In the previous metadynamics study[21], the free energy of the two states was found to be comparable and the highest free energy barrier between the two states was also low, however they did not observe spontaneous collapse of Gly rich loop in 40 ns simulation. Here, in longer time scale simulation (600 ns) of ApoCK2α we were not only able to observe both the states but also conclude that the collapsed state is equally probable, if not preferred, to occur in solution over the stretched conformation.

Dynamics reveals a conformational state of hinge/αD region distinct from that prevalent in crystal structures

For the analysis of conformational heterogeneity of the hinge/αD region we chose distance between the COMs of Phe121 and Val162 (dist121-162), and dihedral angle C-Cα-Cβ-Cγ of Phe 121 (dihed121) as reaction coordinates and calculated the FEL (Figure 5).

The first important observation about the conformations of the hinge/αD region is that they deviate considerably from the conformations observed in the crystal structures. As

described in the earlier section, most of the crystal structures exhibit two types of hinge/αD conformations- closed and open (Figure 2B). However, the energy landscape for the hinge/αD conformations sampled in the molecular dynamics simulations demonstrates one deep minimum and three comparatively shallower minima, both in the ApoCK2α and CXCK2α simulation (Figure 5A and B). We define them as Min1- with dist121-162 corresponding to ~12 to 14 Å and dihed121 corresponding to ~ -50° to -70° ; Min2- with dist121-162 corresponding to ~12 to 14 Å and dihed121 corresponding to ~ 50° to 70° ; Min 3- with dist121-162 corresponding to ~8 to 10 Å and dihed121 corresponding to ~ 50° to 70° ; and Min4- with dist121-162 corresponding to ~8 to 10 Å and dihed121 corresponding to ~ 140° to 180°. This points towards multiple hinge/αD region conformations existing in dynamic equilibrium. We extracted the representative structures from each of the minima and compared them (Figure 5C). The FELs in both ApoCK2α and CXCK2α reveal the stable conformations of hinge/αD region that are distinct from those observed in crystal structures determined so far. The deep minimum on FEL (Min 3) with the lowest energy corresponds to a state in which the Phe121 is partially buried in the hydrophobic cavity and the distance between the αD helix and β7 is similar to that found in the open conformation structure (Figure 5C). This is the most populated state found in the dynamics.

The description of the functional states for the protein kinases have incorporated the concept of Catalytic-spine (C-spine) and Regulatory-spine (R-spine)[24, 48]. These are group of conserved hydrophobic residues in kinases that occur contiguously in the protein kinases and are assembled in the active state of the enzyme. Considering the constitutively active state of the CK2α, it was presumed that the C-spine as well as R-spine would be well formed as in the active form of other protein kinases. However, in case of CK2α, although R-spine, comprising of residues Leu85, Leu97, His154, trp176 and Asp214 was found to be structurally assembled in crystal structures, the C-spine, formed by Val53, Vl66, Phe121, Val162, Met163, Ile164,

Met221 and Met225 was found to be ambiguous (Figure 6). The source of this ambiguity is the dismantled C-spine observed in the open hinge/αD (hitherto assumed to be functional) state with Phe121 pointing outward and assembled C-spine in the closed but non-functional state, with Phe121 embedding the hydrophobic cavity[22, 24]. The analysis of structures representing the deepest minimum in the FEL corresponding to the hinge/αD region in this work, revealed that R-spine was well formed in all the structures and the C spine is formed in most of the structures (Figure 6).

Recently, novel inhibitors targeting the cavity near the αD helix have been discovered[14]. The hinge/αD region conformation of several of these complex structures resembles the one found in the lowest minimum. This suggests that the inhibitors described in the work by Brear et al.[14] target this particular conformation. From the analyses mentioned above, we conclude that there exists an equilibrium between the hinge/αD conformation with partially buried Phe121 side chain along with comparable distance between αD and β7 to that found in crystal structures and an outward open Phe121 side chain with the longer distance between αD and β7.

Furthermore, during the long timescale dynamics (1.2 μs) of either ApoCK2α or CXCK2α, closed state of hinge/αD was not observed, further emphasizing the effect of external factors like crystallization conditions and nature of ligands, on the determination of this conformation in crystal structures.

Inhibitor does not affect the hinge/αD region dynamics

Another interesting observation from the simulations is that the presence of inhibitor does not significantly affect the hinge/αD region dynamics and the difference in the dynamics is much more subdued as compared to the Gly-rich loop. This is evident from both the RMSF values (Cyan and Purple shaded regions in Figure 3B) and the FEL plots (Figure 5A and B).

The FEL for CXCK2α, differs only slightly with ApoCK2α. The region on the FEL corresponding to the "open" state structures as described in the Figure 2B, is almost unoccupied in ApoCK2α simulations (Figure 5A, black ellipse) whereas there are few frames that show the hinge/αD state corresponding to that region, in CXCK2α simulations (Figure 5B, black ellipse) This is further evident in the Principal Component Analysis presented in the next section.

Principal Component Analysis highlights the difference in the dynamics of ApoCK2α and CXCK2α

The results described above indicate that simulating the dynamics of the CK2α captures the conformational landscape of the enzyme unexplored by the crystal structures determined till now. Additionally, we have observed crucial differences in the dynamics between ApoCK2α and CXCK2α. However, owing to high dimensionality of these systems, gaining insight into the specific motions leading to the differences in the dynamics becomes difficult. Principal Component Analysis alleviates this problem by reducing the dimensionality of the system and highlighting only the dominant motions in the protein[49]. PCA was performed on the Cα atom coordinates for entire trajectory of each system. Prior to the calculation of covariance matrix, both the trajectories were fitted to the Apo crystal structure. First five Principal Components (PC) explain 80.7 % and 79.2 % variance in ApoCK2α and CXCK2α trajectories respectively. The motion along the first PC is relatively dominant in both the trajectories with 51.1 % and 62.7 % contribution to total variance in ApoCK2α and CXCK2α respectively.

The motion along the first PC in both the systems corresponds primarily to the shearing motion between the two domains. The β4/β5 loop stretches with the outward movement of the αD helix. Simultaneously, the C-terminal domain including αF and αGH2 helices moves in

opposite direction giving rise to shearing motion (Figure S2A). The motion along the second PC corresponds to the opening and closing of the two lobes around active site. This mostly incorporates the collapse and stretching of Gly-rich loop. In concert with the results obtained from the FEL, motion along this PC vary in ApoCK2α and CXCK2α. The distance between the Arg47 Cα and His160 Cα are in accordance with the FEL values, with ApoCK2α showing a much wider range as compared to CXCK2α (Figure S2B).

Interestingly, there is little difference in motions along the first PC in ApoCK2α and CXCK2α. Most of the difference between the dynamics of the two systems lies in the second PC. To further explore this, we compared the flexibility of ApoCK2α and CXCK2α along their corresponding first and second PCs (Figure 7).

Along first PC, both the systems show similar fluctuations (Figure 7A) with few differences. β4/β5 loop and the hinge/αD region shows higher fluctuation in the CXCK2α whereas αGH2 show slightly higher fluctuations in ApoCK2α. However, in case of motion along the second PC the flexibility of the Gly-rich loop and surrounding regions is drastically reduced in CXCK2α (Figure 7B). This suggests that the binding of inhibitor restricts opening and closing type motion of the enzyme.

Discussion

Since its discovery, CK2α has been an intriguing protein kinase with its constitutive activity, ubiquitous presence, broad substrate specificity and dual co-substrate utilization. With increasing repertoire of high resolution crystal structures, the remarkable conformational heterogeneity of certain regions further added to the complexity in comprehensive understanding of this molecule (Figure 1). In particular, the remarkable conformational heterogeneity of the hinge/αD region, as compared to its homolog in maize, has led to several studies in pursuit to explore and understand it. We mapped this heterogeneity observed in the

human CK2α structures based on current understanding of the conformational states of the hinge/αD (Figure 2). This mapping primarily corroborates the previous studies that the hinge/αD region takes primarily two conformations- "open" and "closed". Next, we go further, to explore this conformational heterogeneity in solution. Long timescale MD simulations were performed to observe the conformational landscape explored by the enzyme in solution. The simulations revealed much higher conformational variability than that observed in the crystal structure ensemble. Free energy landscape corresponding to the conformations of the hinge/αD region, revealed for the first time that in solution the enzyme is found in dynamic equilibrium between multiple states. The "open" state of hinge/αD prevalent in the crystal structure ensemble is rarely populated in solution. Instead, we determine a novel prevalent state where the Phe121 side chain is partially buried in the hydrophobic cavity (Figure 5). In this state, the catalytic spine presumed to be important in the activity of the enzymes seems less dismantled as compared to the "open" state structures determined so far (Figure 6). This corroborates the observations made in previous studies, based on the numerous crystal structures obtained in different conditions, that the hinge/αD region is in dynamic equilibrium between different conformational states and this equilibrium shifts in response to external factors. However, for the inhibitor (CX-4945), studied in this work, we do not observe any such shift in the equilibrium towards a particular conformation of hinge/αD region (Figure 5). This provides us with two novel insights regarding hinge conformation. Firstly, hinge can take multiple conformations and not just the "open" and "closed" conformations observed in the crystal structures. Secondly, the inhibitor CX4945 does not influence this equilibrium and consequently dynamics of hinge region. A comparison of the dynamics of ApoCK2α with CXCK2α further revealed quenching of the overall dynamics of the enzyme in inhibitor bound state (Figure 3). This observation has also been made previously in case of PKA[47] and shift in the dynamic equilibrium between different states is a viable mechanism in this constitutively

active protein kinase. We observe this shift in equilibrium in the conformation of the Gly-rich loop which also exists in dynamic equilibrium between two states in Apo form (Figure 4).

The results presented in this work provide novel insight into the conformational heterogeneity of the catalytic subunit of the CK2 and underline the importance of dynamics of enzyme in the solution state. The recent discovery of hinge pocket binding inhibitors[14] and the resemblance of these structures with the most populated hinge/αD conformational state determined in our simulations further paves way to exploit these results in the discovery of novel noncompetitive inhibitors.

Acknowledgement

This work was supported by the Institute of Transformative Bio-Molecules of Nagoya University and also partly supported by Grants-in-Aid for Scientific Research, JSPS KAKENHI Grant Number 26119006, 15K21711 and 17K07305. The authors declare no conflict of interest.

References

1. Manning G, Whyte DB, Martinez. R., Hunter T, Sudarsanam S. The Protein Kinase Complement of the Human Genome. Science 2002;298(5600):1912–1934.
2. Meggio F, Pinna LA. One-thousand-and-one substrates of protein kinase CK2? FASEB J 2003;17(3):349–368.
3. Pinna LA. Protein kinase CK2: a challenge to canons. J Cell Sci 2002;115(20):3873–3878.
4. Ahmed K, Gerber DA, Cochet C. Joining the cell survival squad: an emerging role for protein kinase CK2. Trends Cell Biol 2002;12(5):226–230.

5. Channavajhala P, Seldin DC. Functional interaction of protein kinase CK2 and c-Myc in lymphomagenesis. Oncogene 2002;21(34):5280–5288.

6. Tawfic S, Yu S, Wang H, Faust R, Davis A, Ahmed K. Protein kinase CK2 signal in neoplasia. Histol Histopathol 2001;16(2):573–582.

7. Trembley JH, Chen Z, Unger G, Slaton J, Kren BT, Waes C Van, Ahmed K. Emergence of protein kinase CK2 as a key target in cancer therapy. BioFactors 2010;36(3):187–195.

8. Cozza G. The Development of CK2 Inhibitors: From Traditional Pharmacology to in Silico Rational Drug Design. Pharmaceuticals 2017;10(26):1–23.

9. Niefind K, Guerra B, Ermakowa I, Issinger O-G. Crystal structure of human protein kinase CK2: insights into basic properties of the CK2 holoenzyme. EMBO J 2001;20(19):5320–5331.

10. Boldyreff B, Meggio F, Pinna LA, Issinger OG. Protein kinase CK2 structure-function relationship: effects of the beta subunit on reconstitution and activity. Cell Mol Biol Res 1994;40(5–6):391–399.

11. Therese Lang P, Holton JM, Fraser JS, Alber T. Protein structural ensembles are revealed by redefining X-ray electron density noise. Proc Natl Acad Sci 2014;111(1):237–242.

12. Pierre F, Chua PC, O'Brien SE, Siddiqui-Jain A, Bourbon P, Haddach M, Michaux J, Nagasawa J, Schwaebe MK, Stefan E, Vialettes A, Whitten JP, Chen TK, Darjania L, Stansfield R, Anderes K, Bliesath J, Drygin D, Ho C, Omori M, Proffitt C, Streiner N, Trent K, Rice WG, Ryckman DM. Discovery and SAR of 5-(3-Chlorophenylamino)benzo[*c*][2,6]naphthyridine-8-carboxylic Acid (CX-4945), the First Clinical Stage Inhibitor of Protein Kinase CK2 for the Treatment of Cancer. J Med Chem 2011;54(2):635–654.

13. Raaf J, Guerra B, Neundorf I, Bopp B, Issinger O-G, Jose J, Pietsch M, Niefind K. First structure of protein kinase CK2 catalytic subunit with an effective CK2 beta-competitive ligand. ACS Chem Biol 2013;8:901–907.

14. Brear P, Fusco C De, Hadje Georgiou K, Francis-Newton NJ, Stubbs CJ, Sore H, Venkitaraman A, Abell C, Spring DR, Hyvönen M. Specific inhibition of CK2α from an anchor outside the active site. Chem Sci 2016;7(11):6839–6845.

15. Prudent R, Cochet C. New protein kinase CK2 inhibitors: jumping out of the catalytic box. Chem Biol 2009;16(2):112–120.

16. Battistutta R. Protein Kinase CK2 in Health and Disease:Structural bases of protein kinase CK2 inhibition. Cell Mol Life Sci 2009;66(11–12):1868–1889.

17. Ohno H, Minamiguchi D, Nakamura S, Shu K, Okazaki S, Honda M, Misu R, Moriwaki H, Nakanishi S, Oishi S, Kinoshita T, Nakanishi I, Fujii N. Structure–activity relationship study of 4-(thiazol-5-yl)benzoic acid derivatives as potent protein kinase CK2 inhibitors. Bioorg Med Chem 2016;24(5):1136–1141.

18. Kinoshita T, Sekiguchi Y, Fukada H, Nakaniwa T, Tada T, Nakamura S, Kitaura K, Ohno H, Suzuki Y, Hirasawa A, Nakanishi I, Tsujimoto G. A detailed thermodynamic profile of cyclopentyl and isopropyl derivatives binding to CK2 kinase. Mol Cell Biochem 2011;356(1–2):97–105.

19. Niefind K, Issinger O-G. Conformational plasticity of the catalytic subunit of protein kinase CK2 and its consequences for regulation and drug design. Biochim Biophys Acta - Proteins Proteomics 2010;1804(3):484–492.

20. Niefind K, Raaf J, Issinger O-G. Protein kinase CK2: From structures to insights. Cell Mol Life Sci 2009;66:1800–1816.

21. Gouron A, Milet A, Jamet H. Conformational Flexibility of Human Casein Kinase Catalytic Subunit Explored by Metadynamics. Biophys J 2014;106(5):1134–1141.

22. Battistutta R, Lolli G. Structural and functional determinants of protein kinase CK2α: facts and open questions. Mol Cell Biochem 2011;356(1–2):67–73.

23. Raaf J, Klopffleisch K, Issinger OG, Niefind K. The Catalytic Subunit of Human Protein Kinase CK2 Structurally Deviates from Its Maize Homologue in Complex with the Nucleotide Competitive Inhibitor Emodin. J Mol Biol 2008;377(1):1–8.

24. Bischoff N, Raaf J, Olsen B, Bretner M, Issinger OG, Niefind K. Enzymatic activity with an incomplete catalytic spine: Insights from a comparative structural analysis of human CK2α and its paralogous isoform CK2α. Mol Cell Biochem 2011;356(1–2):57–65.

25. Campbell E, Kaltenbach M, Correy GJ, Carr PD, Porebski BT, Livingstone EK, Afriat-Jurnou L, Buckle AM, Weik M, Hollfelder F, Tokuriki N, Jackson CJ. The role of protein dynamics in the evolution of new enzyme function. Nat Chem Biol 2016;12(11):944–950.

26. Niefind K, Bischoff N, Golub A, Bdzhola V, Balanda A, Prykhod'ko A, Yarmoluk S. Structural Hypervariability of the Two Human Protein Kinase CK2 Catalytic Subunit Paralogs Revealed by Complex Structures with a Flavonol- and a Thieno[2,3-d]pyrimidine-Based Inhibitor. Pharmaceuticals 2017;10(1):9.

27. Freddolino PL, Liu F, Gruebele M, Schulten K. Ten-Microsecond Molecular Dynamics Simulation of a Fast-Folding WW Domain. Biophys J Biophys Lett 2008;108:L75–L77.

28. Durrant JD, Bush RM, Amaro RE. Microsecond Molecular Dynamics Simulations of Influenza Neuraminidase Suggest a Mechanism for the Increased Virulence of Stalk-Deletion Mutants. J Phys Chem B 2016;120:8590–8599.

29. Yu I, Mori T, Ando T, Harada R, Jung J, Sugita Y, Feig M. Biomolecular interactions modulate macromolecular structure and dynamics in atomistic model of a bacterial

cytoplasm. Elife 2016;5:e19274.

30. Sanbonmatsu KY. Computational studies of molecular machines: the ribosome. Curr Opin Struct Biol 2012;22:168–174.

31. Battistutta R, Cozza G, Pierre F, Papinutto E, Lolli G, Sarno S, O'Brien SE, Siddiqui-Jain A, Haddach M, Anderes K, Ryckman DM, Meggio F, Pinna LA. Unprecedented selectivity and structural determinants of a new class of protein kinase CK2 inhibitors in clinical trials for the treatment of cancer. Biochemistry 2011;50(39):8478–8488.

32. Berman HM, Westbrook J, Feng Z, Gilliland G, Bhat TN, Weissig H, Shindyalov IN, Bourne PE. The Protein Data Bank. Nucleic Acid Res 2000;28(1):235–242.

33. Krissinel E, Henrick K. Multiple alignment of protein structure in three dimensions. Lect Notes Comput Sci 2005;3695:67–68.

34. Abraham MJ, Murtola T, Schulz R, Páll S, Smith JC, Hess B, Lindahl E. GROMACS: High performance molecular simulations through multi-level parallelism from laptops to supercomputers. SoftwareX 2015;1:19–25.

35. Wang J, Wolf RM, Caldwell JW, Kollman PA, Case DA. Development and testing of a general amber force field. J Comput Chem 2004;25(9):1157–1174.

36. Wang J, Wang W, Kollman PA, Case DA. Automatic atom type and bond type perception in molecular mechanical calculations. J Mol Graph Model 2006;25(2):247–260.

37. Sousa da Silva AW, Vranken WF. ACPYPE - AnteChamber PYthon Parser interfacE. BMC Res Notes 2012;5(367):1–8.

38. Berendsen HJC, Postma JPM, Gunsteren WF van, DiNola A, Haak JR. Molecular dynamics with coupling to an external bath. J Chem Phys 1984;81(8):3684–3690.

39. Parrinello M, Rahman A. Polymorphic transitions in single crystals: A new molecular dynamics method. J Appl Phys 1981;52(12):7182–7190.

40. Bussi G, Donadio D, Parrinello M. Canonical sampling through velocity rescaling. J Chem Phys 2007;126(1):14101-1–7.

41. Pettersen EF, Goddard TD, Huang CC, Couch GS, Greenblatt DM, Meng EC, Ferrin TE. UCSF Chimera-A visualization system for exploratory research and analysis. J Comput Chem 2004;25(13):1605–1612.

42. Humphrey W, Dalke A, Schulten K. VMD-Visual Molecular Dynamics. J Mol Graph 1996;14:33–38.

43. Guerra B, Bischoff N, Bdzhola VG, Yarmoluk SM, Issinger OG, Golub AG, Niefind K. A Note of Caution on the Role of Halogen Bonds for Protein Kinase/Inhibitor Recognition Suggested by High- and Low-Salt CK2α Complex Structures. ACS Chem Biol 2015;10(7):1654–1660.

44. Schnitzler A, Olsen BB, Issinger OG, Niefind K. The protein kinase CK2Andante holoenzyme structure supports proposed models of autoregulation and trans-autophosphorylation. J Mol Biol 2014;426(9):1871–1882.

45. Klopffleisch K, Issinger OG, Niefind K. Low-density crystal packing of human protein kinase CK2 catalytic subunit in complex with resorufin or other ligands: A tool to study the unique hinge-region plasticity of the enzyme without packing bias. Acta Crystallogr Sect D Biol Crystallogr 2012;68(8):883–892.

46. Seckler JM, Barkley MD, Wintrode PL. Allosteric suppression of HIV-1 reverse transcriptase structural dynamics upon inhibitor binding. Biophys J 2011;100(1):144–153.

47. Masterson LR, Shi L, Metcalfe E, Gao J, Taylor SS, Veglia G. Dynamically committed, uncommitted, and quenched states encoded in protein kinase A revealed by NMR spectroscopy. Proc Natl Acad Sci 2011;108(17):6969–6974.

48. Taylor SS, Kornev AP. Protein kinases: evolution of dynamic regulatory proteins.

Trends Biochem Sci 2011;36(2):65–77.

49. Amadei A, Linssen ABM, Berendsen HJC. Essential dynamics of proteins. Proteins Struct Funct Genet 1993;17:412–425.

Figure Legends

Figure 1 – Five regions of conformational variability in CK2α. A) Residue wise RMSD for Cα atoms of the crystal structures analyzed in this study. The average RMSD has been shown by black line. B) CX4945 bound crystal structure (PDB id 3PE1). Functionally and structurally relevant regions showing high variability are colored

Figure 2 –Two conformational states of the Gly rich loop and hinge region. A) Two extreme conformations of the Gly-rich loop observed in the crystal structures - PDB 3FWQ in grey showing collapsed state and PDB 3PE1 in blue showing stretched state. B) Conformational states of hinge and αD helix region. Plot of the distance between COMs of Phe121 and Val162 versus the dihedral angle C, Cα, Cβ and Cγ of Phe121 for each structure. The two prevalent states defined in previous studies have been encircled. Inset shows the difference in the hinge region of the two states for the encircled structures.

Figure 3 – ApoCK2α shows higher flexibility than CXCK2α. A) Superposed structures of Apo (PDB id 3AT2 shown in Blue) and CX4945 bound CK2α (PDB id 3PE1 shown in wheat). The inhibitor CX4945 has been shown in gray ball and stick representation. B) Root Mean Square Fluctuation (RMSF) of ApoCK2α (Blue curve) and CXCK2α (Red). Shaded regions are same as in Figure 1A.

Figure 4 - Presence of inhibitor shifts the equilibrium to stretched state of Gly rich loop. A) The FEL along the dist47-160 and dihed47-48 in ApoCK2α, showing two minima. Inset shows comparison of the Gly rich loop in representative structures from two minima (Gray for the minima with smaller dist47-160 and blue for the minima with longer dist47-160) in ApoCK2α. Residues Arg47 and His160 have been shown in red and green stick representation respectively. B) The FEL along the dist47-160 and dihed47-48 in CXCK2α, showing single minima. The location of starting crystal structures (PDB:3AT2 and 3PE1) has been mapped on this plot and shown in white crosses.

Figure 5- Dynamics reveals hinge conformations distinct from crystal structures. A) The FEL along the dist121-162 and dihed121 in ApoCK2α, showing multiple minima. Four minima have been marked by numbers. The location of closed and open state structures (as described in Figure 2B) has been mapped on this FEL and shown by green and black ellipses. The 'outlier' crystal structures have been shown by pink crosses and are mainly close to minimum 3. Finally, the starting structures for MD simulations have been shown in black crosses within the black ellipse. B) The FEL along the dist121-162 and dihed121 in CXCK2α. C) Hinge conformations in representative structures from four different minima in the ApoCK2α FEL. Min1 in pink, Min2 in light green, Min3 in gray, Min4 in light blue. Crystal structure CXCK2α has been shown in red

Figure 6 - Catalytic-spine and Regulatory spine comparison between the crystal structure and structure extracted from dynamics. Residues in Red and Blue show the C-spine and R spine respectively in CX4945 bound crystal structure. Corresponding residues for the representative structure from the most populated state have been shown in the tan (C-spine) and gray (R spine).

Figure 7 - Difference in dominant motions in ApoCK2α and CXCK2α. A) The RMSF along first PC in ApoCK2α (Blue) and CXCK2α (Red). B) The RMSF along second PC in ApoCK2α (Blue) and CXCK2α (Red).

Figures

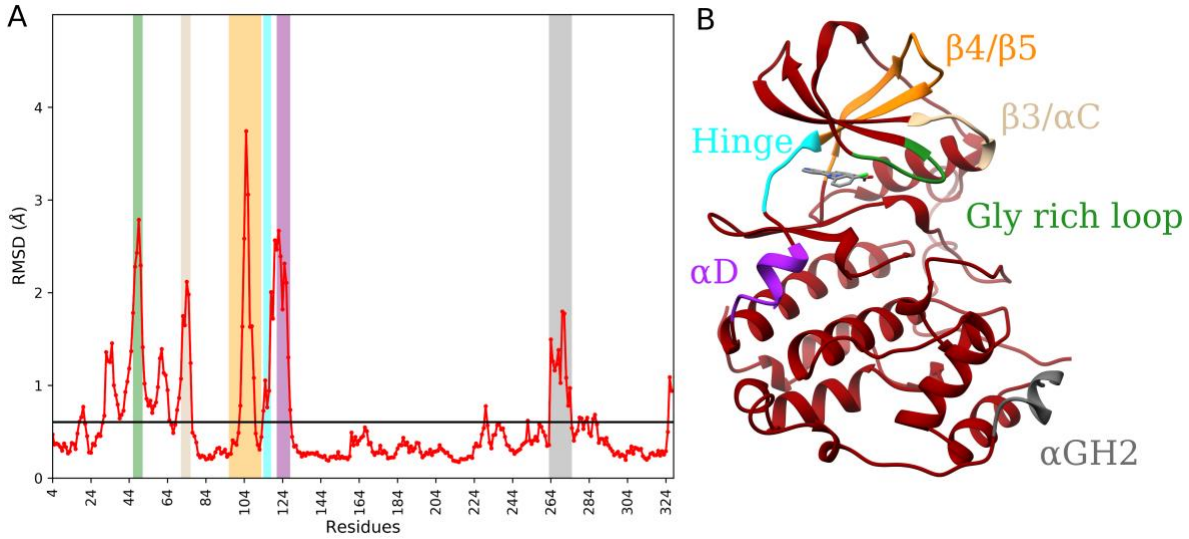

Figure 1 - Five regions of conformational variability in CK2α. A) Residue wise RMSD for Cα atoms of the crystal structures analyzed in this study. The average RMSD has been shown by black line. B) CX4945 bound crystal structure (PDB id 3PE1). Functionally and structurally relevant regions showing high variability are colored

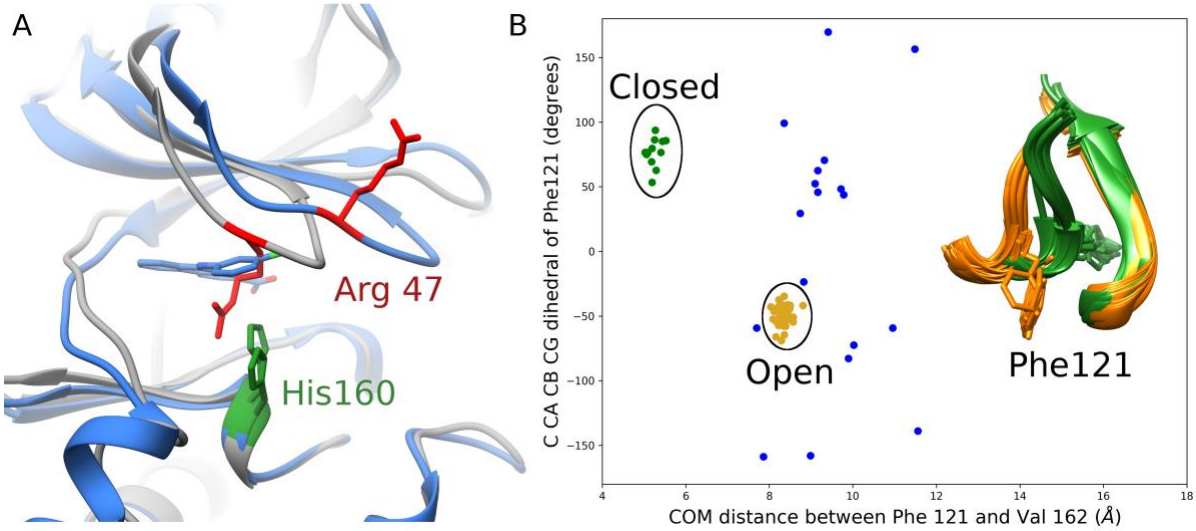

Figure 2–Two conformational states of the Gly rich loop and hinge region. A) Two extreme conformations of the Gly-rich loop observed in the crystal structures - PDB 3FWQ in grey showing collapsed state and PDB 3PE1 in blue showing stretched state. B) Conformational states of hinge and αD helix region. Plot of the distance between COMs of Phe121 and Val162 versus the dihedral angle C, Cα, Cβ and Cγ of Phe121 for each structure. The two prevalent states defined in previous studies have been encircled. Inset shows the difference in the hinge region of the two states for the encircled structures.

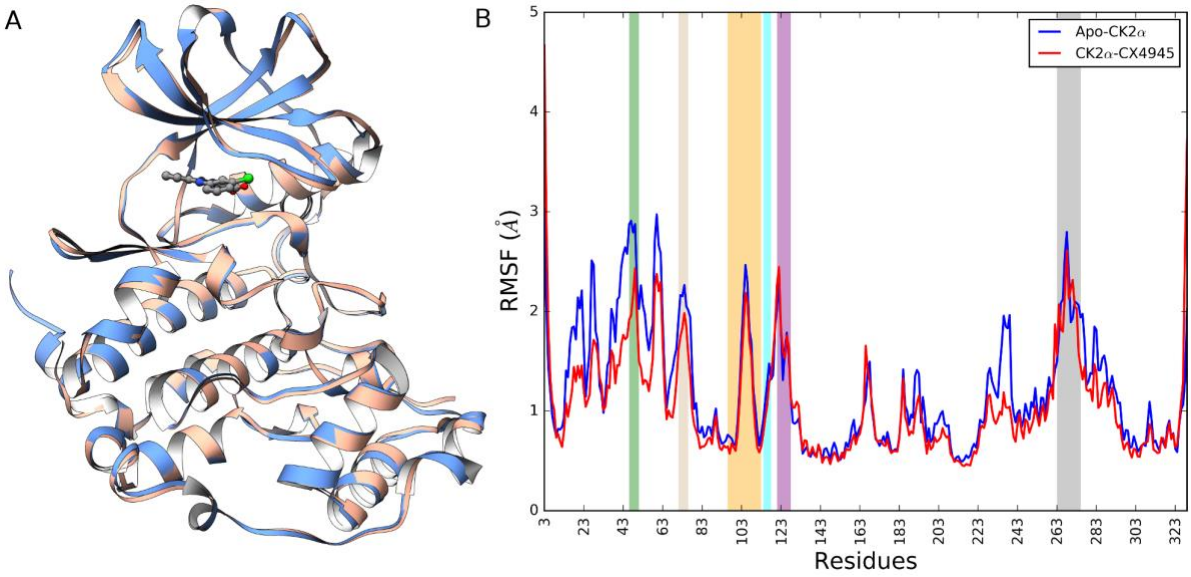

Figure 3– ApoCK2α shows higher flexibility than CXCK2α. A) Superposed structures of Apo (PDB id 3AT2 shown in Blue) and CX4945 bound CK2α (PDB id 3PE1 shown in wheat). The inhibitor CX4945 has been shown in gray ball and stick representation. B) Root Mean Square Fluctuation (RMSF) of ApoCK2α (Blue curve) and CXCK2α (Red). Shaded regions are same as in Figure 1A.

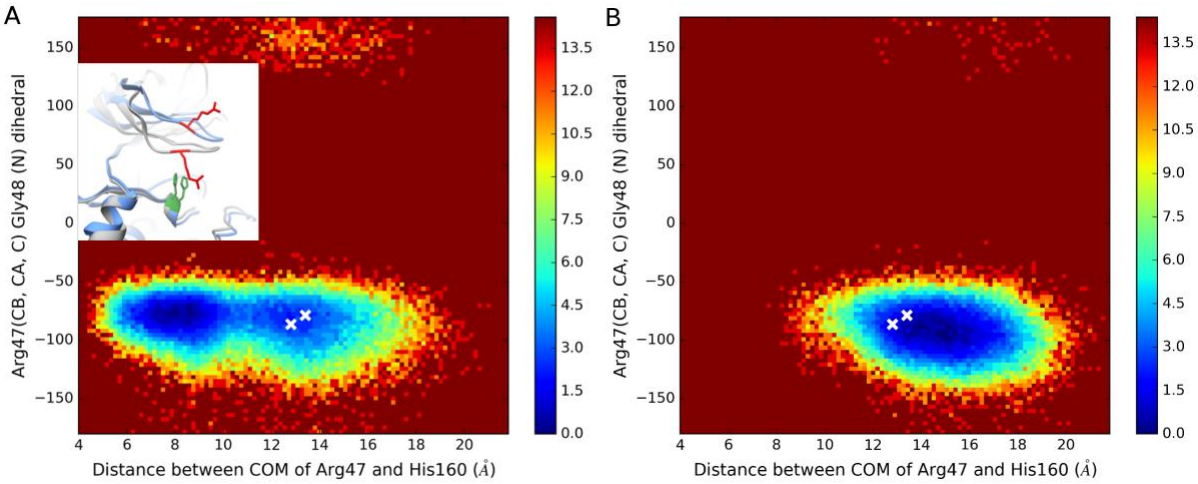

Figure 4- Presence of inhibitor shifts the equilibrium to stretched state of Gly rich loop. A) The FEL along the dist47-160 and dihed47-48 in ApoCK2α, showing two minima. Inset shows comparison of the Gly rich loop in representative structures from two minima (Gray for the minima with smaller dist47-160 and blue for the minima with longer dist47-160) in ApoCK2α. Residues Arg47 and His160 have been shown in red and green stick representation respectively. B) The FEL along the dist47-160 and dihed47-48 in CXCK2α, showing single minima. The location of starting crystal structures (PDB:3AT2 and 3PE1) has been mapped on this plot and shown in white crosses.

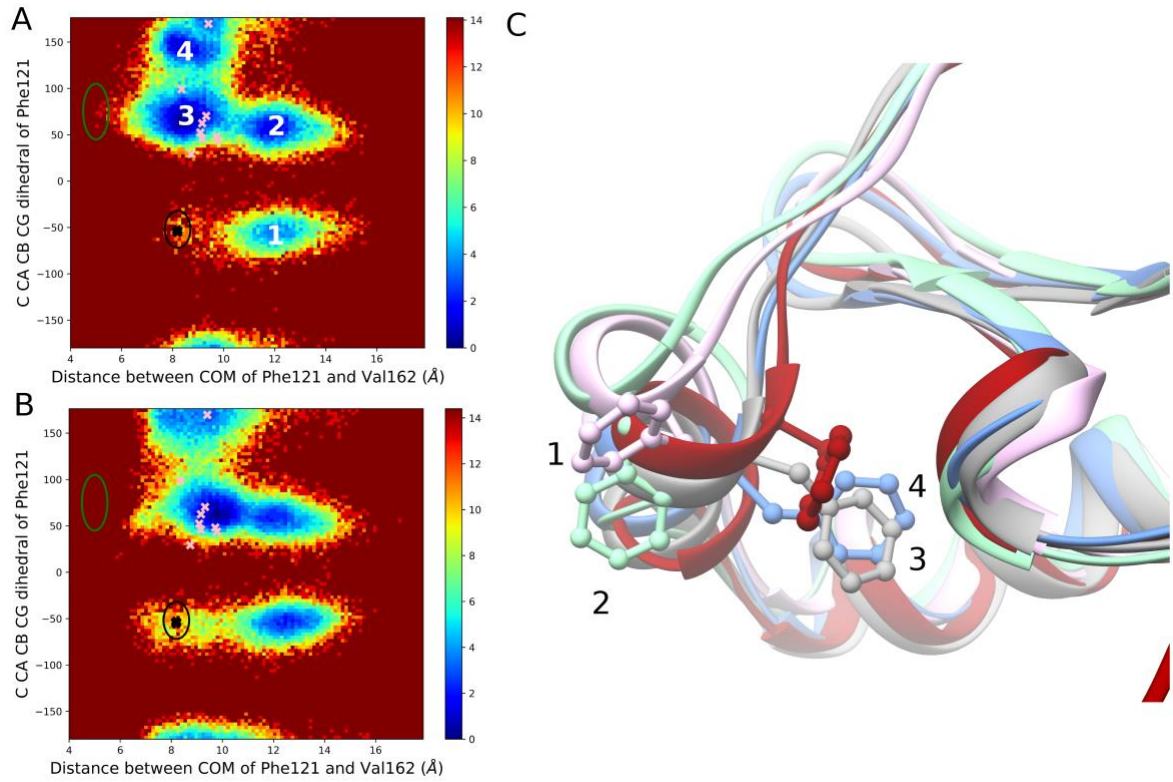

Figure 5- Dynamics reveals hinge conformations distinct from crystal structures. A) The FEL along the dist121-162 and dihed121 in ApoCK2α, showing multiple minima. Four minima have been marked by numbers. The location of closed and open state structures (as described in Figure 2B) has been mapped on this FEL and shown by green and black ellipses. The 'outlier' crystal structures have been shown by pink crosses and are mainly close to minimum 3. Finally, the starting structures for MD simulations have been shown in black crosses within the black ellipse. B) The FEL along the dist121-162 and dihed121 in CXCK2α. C) Hinge conformations in representative structures from four different minima in the ApoCK2α FEL. Min1 in pink, Min2 in light green, Min3 in gray, Min4 in light blue. Crystal structure CXCK2α has been shown in red

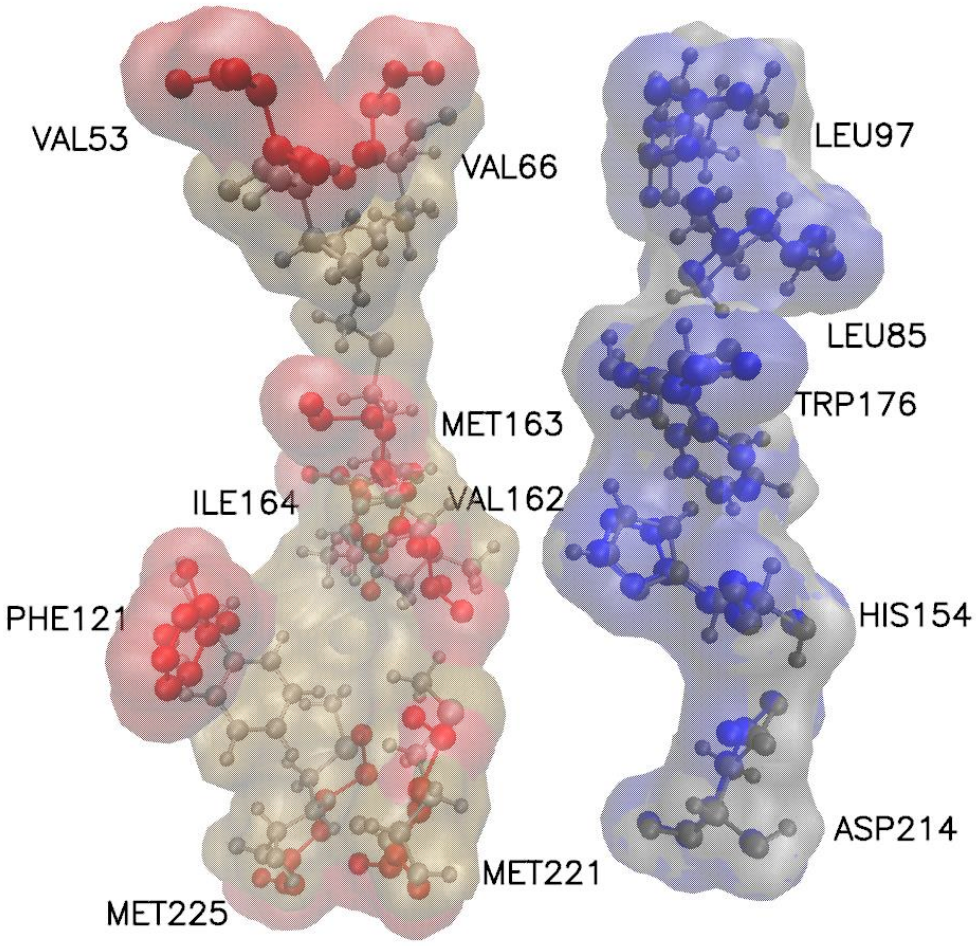

Figure 6 - Catalytic-spine and Regulatory spine comparison between the crystal structure and structure extracted from dynamics. Residues in Red and Blue show the C-spine and R spine respectively in CX4945 bound crystal structure. Corresponding residues for the representative structure from the most populated state have been shown in the tan (C-spine) and gray (R spine).

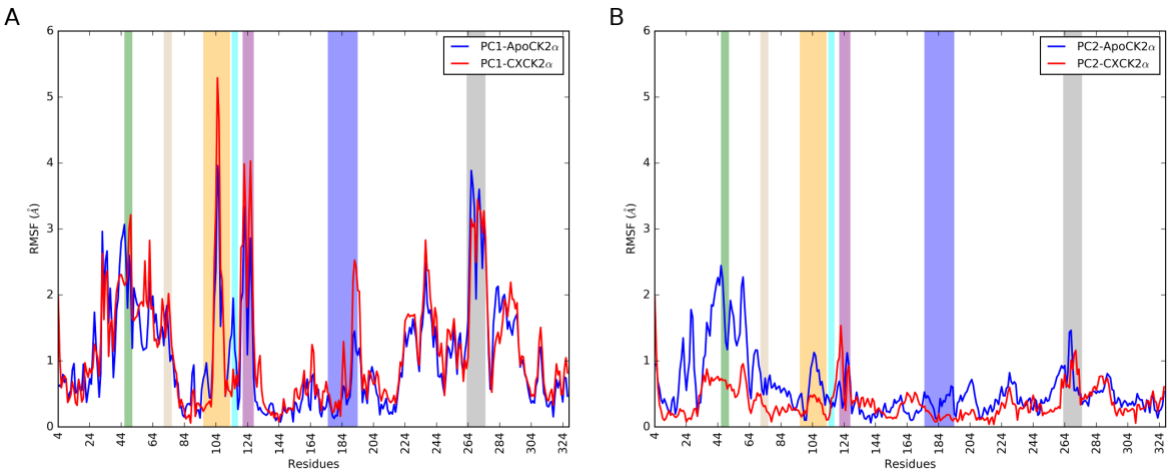

Figure 7- Difference in dominant motions in ApoCK2α and CXCK2α. A) The RMSF along first PC in ApoCK2α (Blue) and CXCK2α (Red). B) The RMSF along second PC in ApoCK2α (Blue) and CXCK2α (Red).